would be in the value of ϵ_H. If we chose $\epsilon_H \cong -0.15$ eV, then excellent agreement with experimental results would be obtained in that the theoretical total energy distribution would then have a peak at about the same energy as that observed by Swanson and Crouser.[10] Since we do not really know what ϵ_H is, however, and because of the approximations mentioned above, this result must be treated with reservation. Also, the accuracy of this procedure for estimating ϵ_H depends on the approximations mentioned above.

The modifications suggested by Gadzuk and improvements in our band-structure model might result in better agreement with the experimental results. However, in view of the doubtful accuracy of the WKB approximation as applied to this problem and the validity of separating the energy of an incident electron into transverse and normal part for any but a parabolic energy band, a different approach would seem to be more promising, e.g., the formulation of the problem in terms of scattering theory or more exact treatment of tunneling from periodic structures in a WKB approximation.[26]

ACKNOWLEDGMENTS

We are grateful to Professor T. E. Feuchtwang and Dr. W. Gadzuk for helpful conversations.

[26] T. E. Feuchtwang, Phys. Rev. (to be published).

PHYSICAL REVIEW VOLUME 186, NUMBER 3 15 OCTOBER 1969

Fourier-Series Representation of the Pt Fermi Surface*

J. B. KETTERSON, F. M. MUELLER, AND L. R. WINDMILLER
Argonne National Laboratory, Argonne, Illinois 60439
(Received 24 April 1969)

The Fourier-series representation is shown to give an accurate representation of the band structure of transition metals in a restricted energy interval, e.g., near the Fermi energy. A 19-term fit to the fifth and sixth bands in fcc Pt is used to compute the de Haas–van Alphen areas and effective masses of all orbits expected for the Fermi surfaces associated with these bands.

INTRODUCTION

MANY methods may be used to calculate energy bands in metals through the entire Brillouin zone and over all energies of interest. The interpretation of various experimental quantities in terms of these energy bands is complicated. Most quantities that can be determined experimentally are averages over some region of momentum space and/or energy. If such averages are found from quantities derived directly from band calculations, much computer time is expended. Even with the comparatively fast interpolation techniques[1] the process requires considerable computational time.

For many properties, e.g., transport phenomena, all that is required is a knowledge of the band structure (momenta and velocities) in the immediate vicinity of the Fermi surface. Even in such a restricted energy range, the time required to derive momenta and velocities ($\nabla_k E$) from the band-structure calculations is substantial. Therefore, a parametrization scheme is required capable of giving a faithful representation of the constant-energy surfaces near the Fermi energy using relatively little computational time. Moreover, experimental momenta and velocities are modified by many-body effects. A properly constructed scheme should have sufficient generality to include such effects.

Such a representation is particularly useful in converting the extremal areas and effective masses measured in de Haas–van Alphen experiments into Fermi momenta (radii) and Fermi velocities. The inverse process of comparing the results of band-structure calculations with experiment is also of interest. For closed, single-valued surfaces possessing inversion symmetry, the problem of converting areas and masses into radii and velocities has been solved by the present authors.[2–4] The problem has also been treated by Foldy.[5] The techniques make use of a series expansion of a theorem due to Lifshitz and Pogorelov.[6] The terms in the series are appropriate combinations of spherical harmonics such that the point-group symmetry of the surface is maintained in each order of the expansion.

One of the surfaces to be discussed here is the open fifth-band hole surface of Pt. This surface, because it is open, does not satisfy the conditions for application of the Lifshitz-Pogorelov theorem. The proper representa-

* Work performed under the auspices of the U. S. Atomic Energy Commission.

[1] F. M. Mueller, Phys. Rev. **153**, 659 (1967).

[2] F. M. Mueller, Phys. Rev. **148**, 636 (1966).

[3] F. M. Mueller and M. G. Priestley, Phys. Rev. **148**, 638 (1966).

[4] J. B. Ketterson, L. R. Windmiller, S. Hornfeldt, and F. M. Mueller, Solid State Commun. **6**, 851 (1968).

[5] L. L. Foldy, Phys. Rev. **170**, 670 (1968).

[6] I. M. Lifshitz and A. V. Pogorelov, Dokl. Akad. Nauk SSSR **96**, 1143 (1954).

tion of an open surface requires an expansion which is invariant under the operations of the space group, i.e., it must be invariant under translations by reciprocal-lattice vectors in addition to the point-group rotations.

FOURIER-SERIES REPRESENTATION

A representation of the energy bands which is invariant under the space group has been given by Wannier.[7] This representation may be viewed as a three-dimensional Fourier series of the form

$$E_n(\mathbf{k})=\sum_{\mathbf{R}} C_{\mathbf{R}}{}^n e^{i\mathbf{k}\cdot\mathbf{R}}, \tag{1}$$

where E_n is the energy of the nth band or sheet of the surface. The vectors $\mathbf{R}$ of the real lattice are generated from the primitive Bravais lattice vectors $\mathbf{a}$, $\mathbf{b}$, and $\mathbf{c}$ by

$$\mathbf{R}=l\mathbf{a}+m\mathbf{b}+n\mathbf{c}, \tag{2}$$

where l, m, and n are integers. We also require a representation of the velocity $\mathbf{v}=\nabla_{\mathbf{k}}E$, i.e.,

$$\mathbf{v}_n=\sum_{\mathbf{R}} i\mathbf{R}C_{\mathbf{R}}{}^n e^{i\mathbf{k}\cdot\mathbf{R}}. \tag{3}$$

The energy is of course a real function of $\mathbf{k}$. Since most crystals of interest have inversion symmetry, the series (1) reduces to a cosine series. However, we will show shortly that it is important from a computational point of view to keep the complex exponential form. Since the energy $E_n(\mathbf{k})$ belongs to the identity representation of the space group, the $C_{\mathbf{R}}{}^n$ are not all independent, but fall naturally into sets in which the value of $C_{\mathbf{R}}{}^n$ is the same for each member of a given set. In analogy with the case of the reciprocal lattice, the set of vectors $\mathbf{R}$ having a common $C_{\mathbf{R}}{}^n$ is called the star of the vector. The vectors $\mathbf{R}$ associated with a given star all transform into one another under the operations of the point group. All $C_{\mathbf{R}}{}^n$ associated with vectors $\mathbf{R}$ of different length must fall, therefore, into different sets or, equivalently, different stars. The converse need not be true in crystals of high symmetry, i.e., coefficients $C_{\mathbf{R}}{}^n$ associated with vectors of the same length are not necessarily in the same star. In the fcc structure, for example, the vectors $\mathbf{R}=\frac{1}{2}\hat{\imath}+\frac{1}{2}\hat{\jmath}+2\hat{k}$, and $\mathbf{R}=\frac{3}{2}\hat{\imath}+\frac{3}{2}\hat{\jmath}$ (in units of the lattice constant a) have the same length but belong to different stars. One should thus factor the summation over $\mathbf{R}$ in Eq. (1) into a double summation over stars and star elements. We define the sum

$$S_j(\mathbf{k})=\sum_{\mathbf{R}\text{ in }j\text{th star}} e^{i\mathbf{k}\cdot\mathbf{R}}$$

or

$$E_n(\mathbf{k})=\sum_j C_j{}^n S_j(\mathbf{k}). \tag{1'}$$

In practice, Eq. (1) is restricted to a finite number of terms. In order that the final representation have the proper symmetry, it is necessary that all elements of a given star be included, i.e., that Eq. (1′) be used. One would then include stars of increasing length until a satisfactory representation of the energy bands (in some interval) was achieved.

TABLE I. Classification of star elements under cubic group.

Type	Degeneracy
000	1
$a00$	6
$aa0$	12
aaa	8
$ab0$	24
aab	24
abc	48

COMPUTATIONAL TECHNIQUES

The Fourier-series technique has been effectively used by Roaf[8] to construct the Fermi surface of the noble metals Cu, Ag, and Au from the dHvA measurements of Shoenberg.[9] Some of the computational techniques developed by Roaf were also used in the present investigation. The Fermi surface of copper is quite close to being spherical, and it was possible to obtain a reasonably accurate representation using only a six-star fit. The sixth-band electron surface of Pt is considerably distorted from a sphere, while the open fifth-band hole surface bears no resemblance to a sphere whatever. It is expected that a faithful representation of the Fermi surface in Pt would require a much larger number of stars, and therefore computational efficiency is of the utmost importance.

We will deal first with the problem of factoring the summation over $\mathbf{R}$ into the double summation over stars and star elements. We begin by generating an array of real lattice vectors $\mathbf{R}(l,m,n)$ with l, m, n assuming all permutations of integers from $-N$ to $+N$. The value of N must be large enough to include all vectors contained within the largest star used. As remarked earlier, in a crystal of low symmetry the elements of a given star can be identified by comparing the lengths of the vectors in the array, i.e., the values of $R^2=R_x{}^2+R_y{}^2+R_z{}^2$; those with the same R^2 are in the same star. In crystals of high symmetry such as fcc, an additional test is required. If we compare the absolute value of the largest component of the vector, we may distinguish between stars the length of whose vectors is degenerate. An alternative test which may be applied is to compare $|R_x|^3+|R_y|^3+|R_z|^3$.

For the remainder of this paper we will confine ourselves to the fcc lattice. The vectors of the real-space lattice are of the seven different types listed in Table I together with the number of vectors in the star.

Table II lists the first 21 stars of the fcc lattice. We have included the length of the vectors in the star, the

[7] G. H. Wannier, Phys. Rev. **52**, 191 (1937).

[8] D. J. Roaf, Phil. Trans. Roy. Soc. London **A255**, 135 (1962).

[9] D. Shoenberg, Phil. Trans. Roy. Soc. London **A255**, 85 (1962).

TABLE II. Stars of the fcc lattice.

Star	$R_x^2+R_y^2+R_z^2$	$R_i^{\max}$	No. of elements	Fundamental vector
1	0	0	1	0
2	$\frac{1}{2}$	$\frac{1}{2}$	12	$\frac{1}{2}\hat{\imath}+\frac{1}{2}\hat{\jmath}$
3	1	1	6	$\hat{\imath}$
4	$\frac{3}{2}$	1	24	$\frac{1}{2}\hat{\imath}+\frac{1}{2}\hat{\jmath}+\hat{k}$
5	2	1	12	$\hat{\imath}+\hat{\jmath}$
6	$\frac{5}{2}$	$\frac{3}{2}$	24	$\frac{1}{2}\hat{\imath}+\frac{3}{2}\hat{\jmath}$
7	3	1	8	$\hat{\imath}+\hat{\jmath}+\hat{k}$
8	$\frac{7}{2}$	$\frac{3}{2}$	48	$\frac{1}{2}\hat{\imath}+\hat{\jmath}+\frac{3}{2}\hat{k}$
9	4	2	6	$2\hat{\imath}$
10	$\frac{9}{2}$	$\frac{3}{2}$	12	$\frac{3}{2}\hat{\imath}+\frac{3}{2}\hat{\jmath}$
11	$\frac{9}{2}$	2	24	$\frac{1}{2}\hat{\imath}+\frac{1}{2}\hat{\jmath}+2\hat{k}$
12	5	2	24	$\hat{\imath}+2\hat{\jmath}$
13	$\frac{11}{2}$	$\frac{3}{2}$	24	$\hat{\imath}+\frac{3}{2}\hat{\jmath}+\frac{3}{2}\hat{k}$
14	6	2	24	$\hat{\imath}+\hat{\jmath}+2\hat{k}$
15	$\frac{13}{2}$	2	48	$\frac{1}{2}\hat{\imath}+\frac{3}{2}\hat{\jmath}+2\hat{k}$
16	$\frac{13}{2}$	$\frac{5}{2}$	24	$\frac{1}{2}\hat{\imath}+\frac{5}{2}\hat{\jmath}$
17	$\frac{15}{2}$	$\frac{5}{2}$	48	$\frac{1}{2}\hat{\imath}+\hat{\jmath}+\frac{5}{2}\hat{k}$
18	8	2	12	$2\hat{\imath}+2\hat{\jmath}$
19	17/2	$\frac{5}{2}$	24	$\frac{3}{2}\hat{\imath}+\frac{5}{2}\hat{\jmath}$
20	17/2	2	24	$\frac{3}{2}\hat{\imath}+\frac{3}{2}\hat{\jmath}+2\hat{k}$
21	9	2	24	$\hat{\imath}+2\hat{\jmath}+2\hat{k}$

magnitude $R_i^{\max}$ of the absolute value of the largest component of the vector, number of elements in the star, and one of the vectors in the star. Observe that stars 10 and 11, 15 and 16, and 19 and 20 are degenerate with respect to length. The value of N used in generating the array was 4 in these calculations. This value of N_{14} is sufficient to generate the first 18 stars together with the 20th. The 19th star will be incomplete. The 19th and 20th stars are degenerate with respect to length, however, and for these reasons we reordered the 19th and 20th stars appearing in Table II for the calculations to be presented in this paper.

Consider next the generation, for a given $\mathbf{k}$, of the energy as given in Eq. (1). We decompose the vector $\mathbf{k}$ into its components along the three primitive vectors of the reciprocal lattice $\mathbf{a}^*$, $\mathbf{b}^*$, and $\mathbf{c}^*$, where $\mathbf{a}^*=\mathbf{b}\times\mathbf{c}/\mathbf{a}\cdot\mathbf{b}\times\mathbf{c}$, etc. Thus $\mathbf{k}=k_a\mathbf{a}^*+k_b\mathbf{b}^*+k_c\mathbf{c}^*$ and the complex exponential becomes (for a given $\mathbf{R}$)

$$e^{i\mathbf{k}\cdot\mathbf{R}}=e^{i(lk_a+mk_b+nk_c)}. \tag{4}$$

The machine programs for calculating transcendental functions run comparatively slowly (approximately 10 times slower than complex double-precision multiplication), so it is important to make minimal use of these subroutines. It is for this reason that the complex exponential representation is preferable to a sine-cosine Fourier representation. In general, we can evaluate (1) by making use of the complex exponential subroutine only three times. All that it is necessary to do is to calculate e^{ik_a}, e^{ik_b}, and e^{ik_c} and then perform repeated complex multiplications, i.e.,

$$e^{i(lk_a+mk_b+nk_c)}=(e^{ik_a}e^{ik_a}\cdots l \text{ times})\times(e^{ik_b}e^{ik_b}\cdots m \text{ times})\times(e^{ik_c}e^{ik_c}\cdots n \text{ times}). \tag{5}$$

These multiplications were carried out in complex double precision, saving considerable time over evaluating (4) directly each time.

Equation (1) is an implicit function of $\mathbf{k}$, and since one usually wants values of $\mathbf{k}$ at fixed energy, it is necessary to use some iterative technique. We have used the Newton-Raphson technique, which was first applied to this problem by Roaf.[8] Consider a vector $\mathbf{k}$ and a closely neighboring vector $\mathbf{k}'=\mathbf{k}+\delta\mathbf{k}$. Using a first-order Taylor expansion, we may relate the energy associated with these two vectors by[10]

$$E(\mathbf{k}+\delta\mathbf{k})\cong E(\mathbf{k})+\nabla E\cdot\delta\mathbf{k}. \tag{6}$$

One important calculation is the cross-sectional area (in momentum space) of the orbit swept out by the motion of an electron on the Fermi surface in a magnetic field. As is well known, the orbit of an electron in a magnetic field $\mathbf{H}$ is given by the intersection of the plane $\mathbf{k}\cdot\hat{H}=k_{\parallel}$ with the Fermi surface, $k_{\parallel}$ being the component of the electron's momentum along $\hat{H}$. If we write $\mathbf{k}(E_F)=k_{\parallel}\hat{H}+\mathbf{k}_{\perp}$, the area of the orbit is given by

$$A=\frac{1}{2}\int_0^{2\pi}k_{\perp}^2(\theta)d\theta, \tag{7}$$

where θ is an angle in the plane of the orbit measured from some convenient reference point. Such integrations are performed accurately and simply using Simpson's rule. In order to accomplish this we must be able to do two things: (1) With both the plane of the orbit and the angle of $k_{\perp}$ in this plane specified (i.e., $k_{\parallel}$ and θ

TABLE III. Interpolation-scheme parameters.

		Parameter (in rydberg a.u.) as calculated in Ref. 11
D bands	d_0	+0.5465
	dd_0	−0.0624
	$dd\pi_1$	+0.0258
	$dd\pi_2$	+0.0196
	$dd\delta$	−0.0003
	γ	+0.0116
Conduction bands	V_{111}	0.0027
	V_{200}	0.0033
Orthogonality	A	1.7822
	LR_0	2.5114
Hybridization	B	2.0984
	LR_1	1.8206
Spin orbit	E_p	0.0214
Fermi energy	E_F	0.6542
Representative error	$\sqrt{\sigma_i^2}$	0.0026[a]

[a] Derived from Fermi surface fit.

[10] It should be emphasized here that this parametrization technique does not attempt to fit all the sheets of the Fermi surface with a single set of parameters C_j^n. Each energy band n defines a sheet of the Fermi surface (or sheets related by the symmetry of the crystal) which is parametrized independently of all the others by its own set of C_j^n. The procedures outlined in this paper are actually applied to each Fermi-surface sheet individually. Thus, when the band index n is omitted in the following sections of this paper, it is to be assumed that only a single band is always being considered.

specified) for some trial vector $\mathbf{k}$, we must have a "return-to-surface" routine. This routine starts from the vector $\mathbf{k}$ and corrects its $k_\perp$ component to generate a new vector which is on the derived energy surface. (2) Having such a correct vector, we must have a "stepping" routine which will change it by a vector $\delta\mathbf{k}$ which is parallel to the surface and in the plane of the orbit (i.e., $\delta\mathbf{k}=\delta k\hat{n}$, where $\hat{n}=\nabla E\times\hat{H}/|\nabla E\times\hat{H}|$) and has a magnitude such that θ will be increased by some specified increment $d\theta$. This new vector will now have the correct values of $k_{||}$ and $\theta+d\theta$ but may need a correction of $k_\perp$ to bring it back to the derived energy surface again. Thus, by alternatively performing the "return-to-surface" and the "stepping" routines we can step around the orbit and perform the Simpson's-rule integration.

Both of the above routines can be conveniently carried out by exploiting Eq. (6). In order to carry out the return-to-surface routine we must replace the vector $\mathbf{k}$ by a new vector $\mathbf{k}'$ given by

$$\mathbf{k}'=\mathbf{k}-\mathbf{k}_\perp(E-E_F)/\nabla E\cdot\mathbf{k}_\perp, \tag{8}$$

where E_F is the energy of the desired shell and E, ∇E, and $k_\perp$ are evaluated at $\mathbf{k}$. To accomplish the stepping routine, the incremental vector $\delta\mathbf{k}=\delta k\hat{n}$ has direction, as above, $\hat{n}=\nabla E\times\hat{H}/|\nabla E\times\hat{H}|$ and magnitude δk found from the solution of the quadratic equation

$$\frac{(\mathbf{k}_\perp+\delta k\hat{n})\cdot\mathbf{k}_s}{|\mathbf{k}_\perp+\delta k\hat{n}||\mathbf{k}_s|}=\cos(\theta+d\theta), \tag{9}$$

where $\mathbf{k}_s$ is the "starting vector" from which the Simpson's-rule integration has begun (i.e., the $k_\perp$ for $\theta=0$). One may also simultaneously calculate the cyclotron effective mass of the orbit using the relation

TABLE IV. Coefficients of the 19-star fit to the sixth band in Pt. $E_F=0.6565$.

Star	Coefficient
1	0.855902
2	−0.061665
3	0.007611
4	0.019434
5	−0.028622
6	−0.013214
7	−0.021314
8	0.001050
9	0.013655
10	−0.004074
11	−0.007675
12	0.000062
13	−0.001328
14	−0.002014
15	−0.000791
16	−0.001946
17	0.000290
18	−0.000081
19	−0.000416

TABLE V. Coefficients of the 19-star fit to the fifth band in Pt, $E_F=0.6565$.

Star	Coefficient
1	−1.29381
2	−1.42782
3	−1.03738
4	−0.75751
5	−0.54141
6	−0.38847
7	−0.28025
8	−0.19179
9	−0.13092
10	−0.09117
11	−0.08814
12	−0.05880
13	−0.03827
14	−0.02357
15	−0.01607
16	−0.01469
17	−0.00533
18	−0.00330
19	−0.00235

$m^*=(1/\pi)(dA/dE)$ in rydberg atomic units, where

$$\frac{dA}{dE}=\int_0^{2\pi}\frac{k_\perp^2}{\mathbf{k}_\perp\cdot\nabla E}d\theta. \tag{10}$$

CALCULATIONS

To generate a Fourier-series representation in the vicinity of the Fermi surface one must have either a band-structure calculation or a set of experimental Fermi-surface data such as dHvA areas and effective masses. For the purpose of this initial investigation it was thought best to use a band-structure calculation rather than dHvA data. This is because it is easier to evaluate the convergence of the series if one can compare directly with radii and velocities rather than areas and effective masses, which might tend to average out distortions of the constant-energy surfaces. The band structure used was the interpolation scheme calcula-

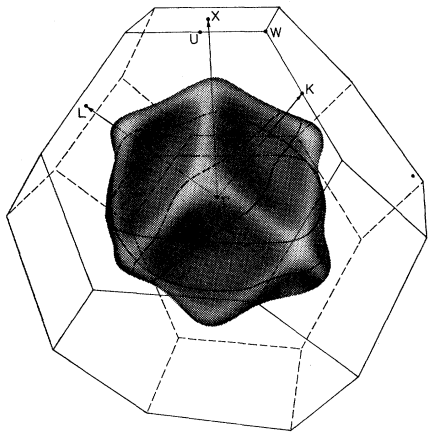

FIG. 1. Sixth-band electron surface in Pt calculated using the interpolation scheme.

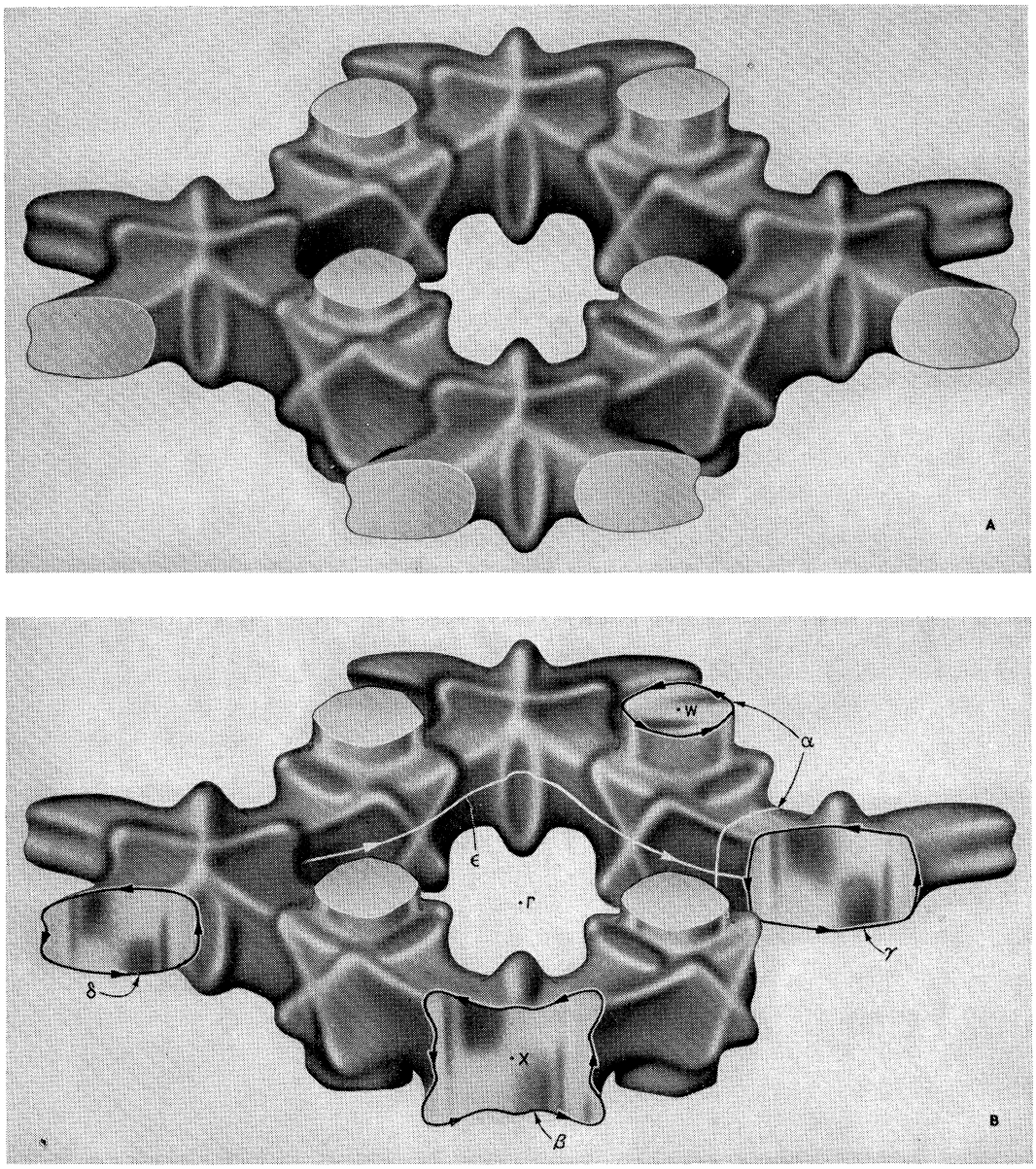

FIG. 2. (a) Open fifth-band hole surface in Pt calculated using the interpolation scheme; (b) open fifth-band hole surface in Pt showing the expected dHvA orbits.

tion of Mueller, Ketterson, Windmiller, and Hörnfeldt.[11] This band structure was derived from both the RAPW calculations of Andersen and Mackintosh[12] and the dHvA measurements of Windmiller and Ketterson.[13] The interpolation-scheme[11] parameters used are given in Table III. Fifty uniformly spaced radii on each of three constant-energy surfaces were generated both for the fifth and sixth bands; the energy on these three surfaces was 0.6465, 0.6565, and 0.6665 Ry. The Fermi energy selected was $E_F=0.6565$ Ry. Equation (1) is a linear equation in the C_j^n when E and $\mathbf{k}$ are given. In order to generate the C_j^n (for each band) we least-squares-fitted all the vectors on the three constant-energy surfaces. Table IV and V give the coefficients C_j^n for a 19-term (star) fit to the sixth- and fifth-band surfaces, respectively. The rms fit to the energy was 0.00064 Ry for the sixth band and 0.0015 Ry for the fifth band. After generating the C_j^n, the k vectors from the band structure were inserted into Eq. (1) and

[11] F. M. Mueller, J. B. Ketterson, L. R. Windmiller, and S. Hörnfeldt (unpublished).
[12] O. K. Andersen and A. R. Mackintosh, Solid State Commun. **6**, 285 (1968).
[13] L. R. Windmiller and J. B. Ketterson, Phys. Rev. Letters **20**, 324 (1968).

iterated back to the corresponding constant-energy shell. The rms change $\delta k/k$ resulting from this process was 0.0032 for the sixth band and 0.012 for the fifth band. A 10-star fit was also carried out. The resulting rms energy was 0.0014 and 0.0035 Ry for the sixth and fifth bands, respectively. The above convincingly shows that a Fourier series can yield an accurate representation of a transition-metal band structure over an energy range of a few hundredths of a rydberg, provided enough stars are included. The calculation of one iteration with 19-term fit takes 0.4 sec on the IBM system 360/50/75 computer of the Argonne Applied Mathematics Division. Usually one iteration is required to return to the surface when going around an orbit. Thus a convergent $\mathbf{k}$ vector can be calculated in less than 1 sec. Our criterion for convergence was $|(E-E_F)k_\perp/\nabla E\cdot\mathbf{k}_\perp|<0.0001$.

Figure 1 shows the sixth-band electron surface together with the fcc Brillouin zone. The [100], [110], and [111] radii of this surface are shown as the dashed portion of the vectors ΓX, ΓK, and ΓL, respectively. Shown also are the [100], [110], and [111] extremal areas in the planes normal to these directions. Figure 2(a) shows the open fifth-band hole surface. This surface has the topology of cylinders extending in the $\langle 100\rangle$ directions and intersecting in pairs at the point X in the zone. Figure 2(b) shows the various extremal orbits expected for this surface. The surface of Fig. 2 is based on an earlier band calculation and is slightly different from the one calculated here. The center of the α orbit is the point W when the field is along the [100] direction and very close to W for a general field direction. The center of the β orbit is at X for all field directions where this orbit exists. The γ orbit is located within the junction formed by the intersection of the "cylinders" and exists for a narrow range of field angles near [110]. The center of this orbit does not lie near any symmetry point, however. The δ orbit also exists for a small range of field angles near [110] but does not lie within the junction. The actual shape of this orbit is somewhat different from that shown in Fig. 2(b). The center of this orbit is also far from any symmetry point. The ϵ orbit runs around the "square" formed by the intersection of the "cylinders." This orbit is centered on the point Γ for all field angles where it exists. The orbits α, γ, and δ have been observed experimentally.[13] Orbits α through δ are holelike in the sense that the area of these orbits decreases with increasing energy. Orbit ϵ is electronlike. Orbits centered on symmetry points are easiest to calculate since the area and effective-mass integrals need be performed only once. For orbits not centered on symmetry points it is necessary to calculate the area and effective mass for several values of $k_{||}$ in order to determine where an extremum is located. After the approximate location of the extremum is found using a coarse mesh on $k_{||}$, the areas and effective masses of three orbits very close to the extremum are calculated. The $k_{||}$ corresponding to the extremal area is then found using quadratic interpolation. The effective mass is then interpolated to the same $k_{||}$.

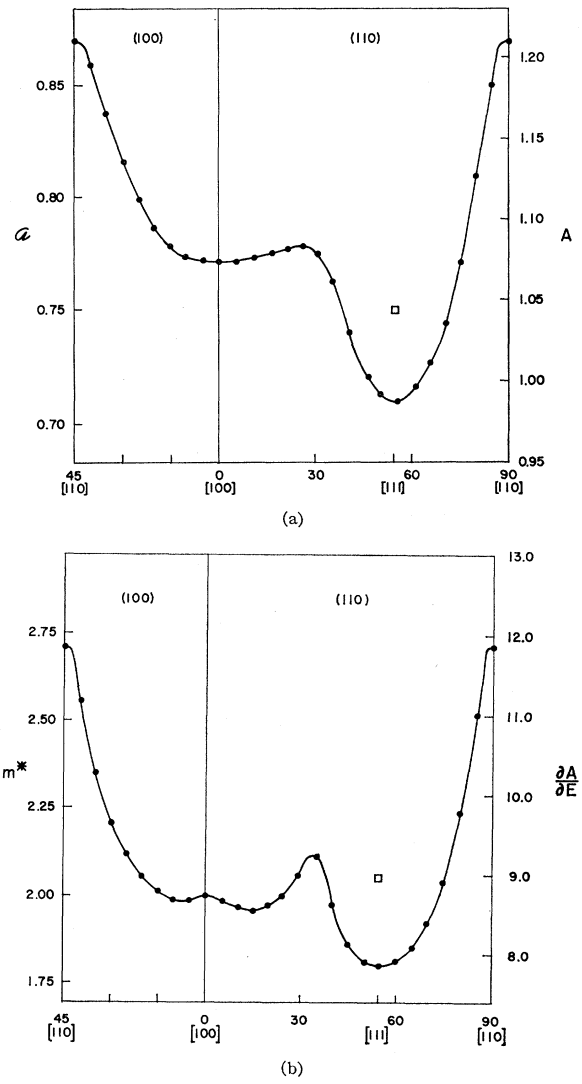

FIG. 3. (a) Calculated dHvA areas for the sixth-band electron surface in the (100) and (110) planes; (b) calculated effective masses for the sixth-band electron surface in the (100) and (110) planes.

The unit of length used in these calculations is $k_{\Gamma X}\equiv 1$. All energies are in rydbergs. Up to this point we have been writing the vector $\mathbf{k}$ as the sum of components perpendicular and parallel to the magnetic field, i.e., $\mathbf{k}_\perp$ and $\mathbf{k}_{||}$ from an origin at the point Γ. However, orbits which do not include the point Γ (e.g., the β orbit) present a special problem since the center for Simpson's-rule integration must be within the orbit. In such cases the center of integration must be moved to a point within the orbit. For the β orbit a convenient center is the point X, and the vector $\mathbf{k}$ can be written as $\mathbf{k}=\mathbf{k}_0+\mathbf{k}_\perp+\mathbf{k}_{||}$, where in this case we set $\mathbf{k}_0=\hat{\imath}+\hat{\jmath}$.

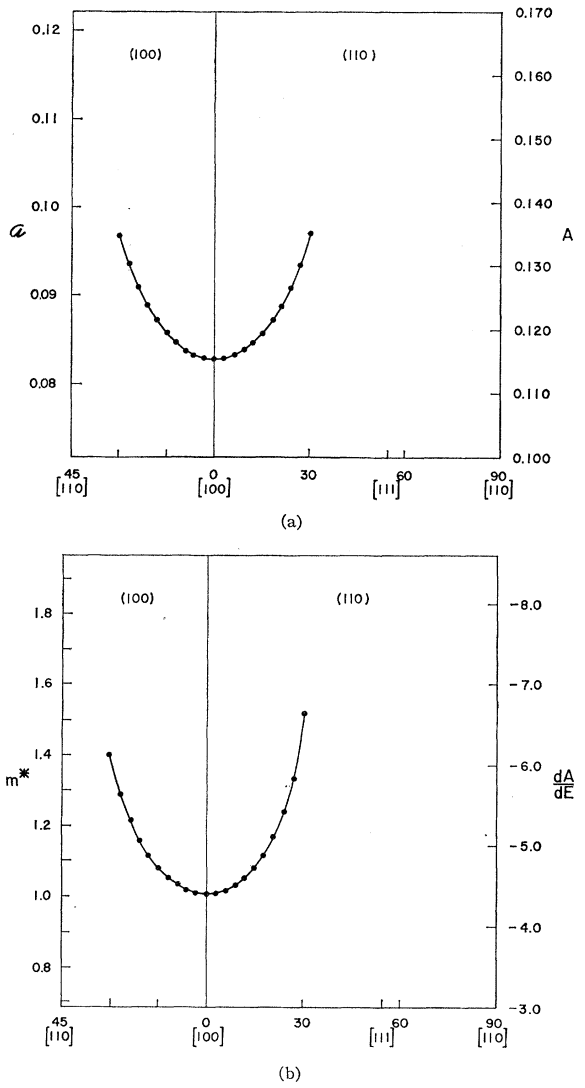

FIG. 4. (a) Calculated dHvA areas for the fifth-band α orbit in the (100) and (110) planes; (b) calculated effective masses for the fifth-band α orbit in the (100) and (110) planes.

Similarly, to compute the α orbit the point W is a convenient origin, so $\mathbf{k}_0=\frac{1}{2}\hat{\imath}+\hat{\jmath}$. The center must also be moved to calculate the γ and δ orbits.

It is also necessary to start the initial iteration(for the first $\mathbf{k}$ vector on the orbit) at a value $\mathbf{k}_s$ which is sufficiently close to the surface that Eq. (6) is approximately valid. If this is not done, the value of $\mathbf{k}$ after iteration may be on a different part of the surface or, alternatively, in a neighboring zone.

dHvA AREAS AND EFFECTIVE MASSES

Figure 3(a) shows the angular dependence of the sixth-band electron dHvA areas calculated for the (100) and (110) planes. The scale at the left of the figure is in the usual atomic units where length is measured in reciprocal Bohr radii. The scale at the right is the one actually used in the calculations. The unit of length is the distance from the center of the zone Γ to the point X. The lone point for $\mathbf{H}\|[111]$ is an off-central orbit. The plane of this orbit does not include the point Γ. This orbit exists for field directions within approximately 20° of [111], ultimately merging with the main branch. The magnitude and angular dependence of the area in the (110) plane are in good agreement with the experiments of Windmiller and Ketterson.[13] Figure 3(b) shows the angular dependence of the effective mass in the (100) and (110) planes. The scale at the left gives the effective mass m^* measured in units of the free-electron mass. The scale at the right is the quantity dA/dE, where dA is in the area units used for the calculation and dE is measured in rydbergs.

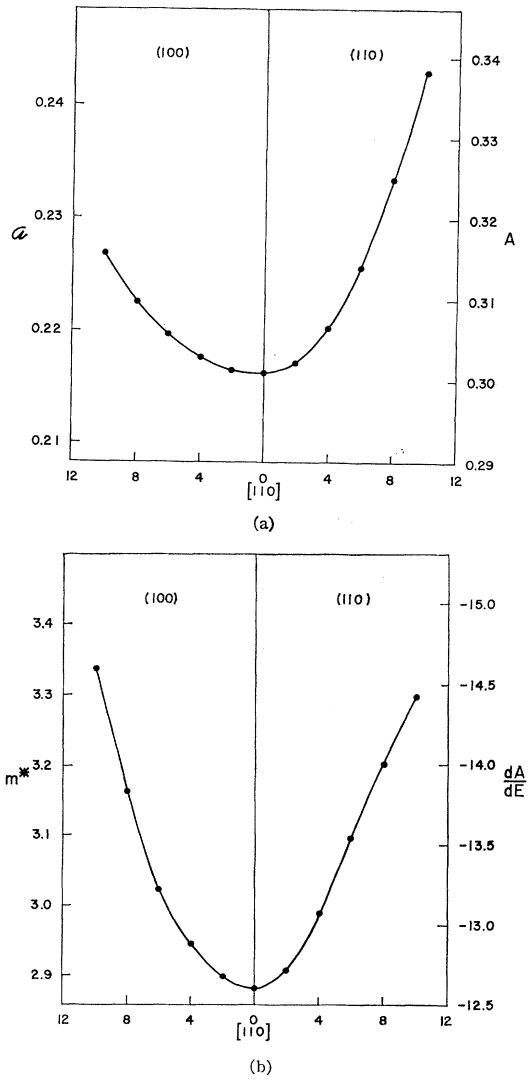

FIG. 5. (a) Calculated dHvA areas for the fifth-band γ orbit in the (100) and (110) planes; (b) calculated effective masses for the fifth-band γ orbit in the (100) and (110) planes.

TABLE VI. Comparison of calculated and experimental areas and masses.

	Direction	Area Theory	Area Expt	Mass Theory	Mass Expt
Electron surface	(100)	0.772	0.778	2.00	2.44
	(110)	0.869	0.865	2.71	3.16
	(111)	0.708	0.695	1.80	2.06
	(111)	0.749	0.725	2.05	2.50
Open-hole surface	(100)α	0.0828	0.0744	1.01	1.53
	(110)β	0.274	···	5.79	···
	(110)γ	0.216	0.218	2.88	3.32
	(110)δ	0.167	0.182	2.77	3.62
	(100)ϵ	1.880	···	4.95	···

The lone point for the field along [111] is the effective mass of the off-central orbit described above. As is well known, the experimental mass will generally be larger than the calculated band mass, because of many-body effects. Thus we cannot compare any of the masses calculated here directly to the experiments of Ketterson and Windmiller.[14] We do expect, however, that the anisotropy of the measured and calculated masses will be similar, since the mass-enhancement effects tend to be isotropic. Every feature, including the "bump" near 30°, is reproduced in the experiments which were carried out in the (110) plane.

We now turn to orbits on the open fifth-band hole surface. Figure 4(a) shows the dHvA areas calculated for the holelike α orbit in the (100) and (110) plane. Calculations were carried out for the field within 30° of [100], although experimentally this orbit exists over a slightly larger angular range. The calculated areas are somewhat larger than the experimentally determined values, but the anisotropy is similar. Figure 4(b) shows the angular dependence of the effective mass of the α orbit. Again, the anisotropy is similar to that observed experimentally. For the field in a (110) plane, symmetry considerations show that the plane of the orbit must include the point W. When the field is tipped away from (100) in an arbitrary direction, that is not necessarily the case. The observed position of minimum area was, however, observed to stay very close to W ($\sim$0.01 unit measured along the X-W line) in the (100) plane. Observe that dA/dE is negative for hole orbits.

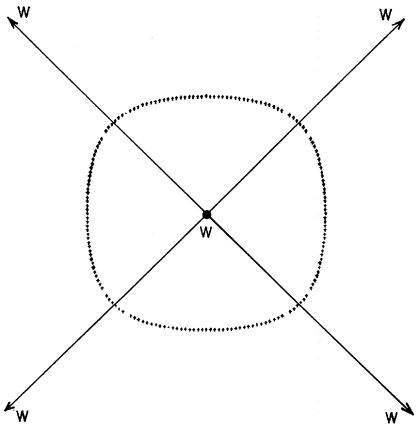

FIG. 6. α orbit for the fifth-band holes with the magnetic field along (100). The orbit is centered on W.

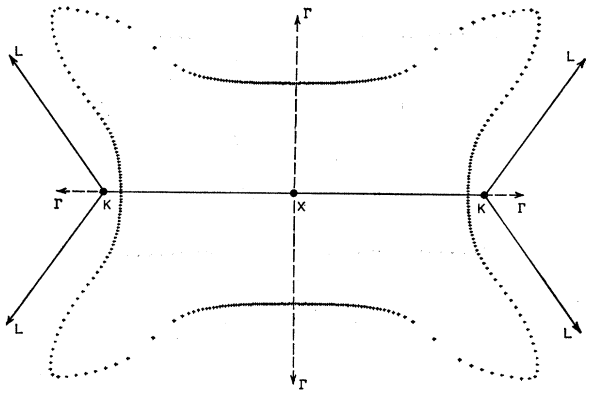

FIG. 7. β orbit for the fifth-band holes with the magnetic field along [100]. The orbit is centered on X.

Figure 5(a) shows the angular dependence of the dHvA area for the γ orbit with the field in the (100) and (110) planes. The orbit exists for the field near [110] and is holelike. The plane of this orbit does not include any symmetry point, so that it is necessary to search for the extremal orbit at each field direction. The γ orbit has been observed experimentally and agrees well with the calculated values. The calculations do not extend over the full angular range for which the orbit exists. Figure 5(b) shows the calculated effective masses for the (100) and (110) planes.

We next discuss the δ orbit which exists for the field near [110]. It was found that for the center of integration on the X-W line, orbits near the position of extremal area could have double-valued radius vectors. However, the radius vector could be made single-valued by moving the integration center off the X-W line. It was further observed that the position of this center had to be changed for different field directions, since otherwise the radii again became double-valued. For this reason few calculations were performed for the δ orbit. For the field in a (100) plane there are two branches for this orbit corresponding to the arms along each of the two ⟨100⟩ axes in this plane. However, in the (110) plane these two branches are degenerate.

The angular dependence of the extremal area and cyclotron effective mass for the β and ϵ orbit was also calculated. Since these orbits have not been observed experimentally, we will not report these results.

In Table VI the measured and calculated values of A and m^* for the magnetic field along the major symmetry directions are given.

[14] J. B. Ketterson and L. R. Windmiller, Phys. Rev. Letters **20**, 321 (1968).

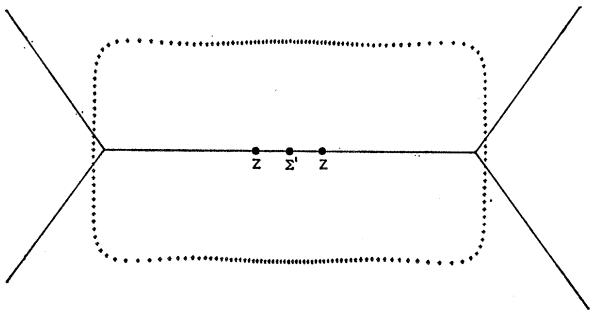

FIG. 8. γ orbit for the fifth-band holes with the magnetic field along [100]. The plane of the orbit intersects the ΓX line 0.126 units from X.

In Figs. 6–9 we show various cross sections of the open-hole surface. Figure 6 shows the α orbit for the field along [100], while Figs. 7 and 8 show the β and γ orbits for the field along [110]. The γ orbit is located 0.126 units away from X along the ΓX line.

INVERSION OF dHvA DATA

We now discuss inversion of dHvA areas and effective masses into radii and velocities. This was first done successfully for the noble metals of Roaf[8] using the Fourier-series representation. Roaf used both a four-star and a six-star representation. Because of the rather large number of terms required to obtain an accurate representation of the Pt Fermi surface, it is essential that the calculations be performed in an economical manner. An inversion of the Pt experimental data has not yet been attempted using the Fourier-series representation but has been accomplished for the Γ-centered surface using the inversion scheme of Mueller.[2–4] Nevertheless, we will discuss how an inversion (using a Fourier series with a large number of stars) could be accomplished. It is our belief that without data on the sensitive ϵ and β orbits an inversion of the open-hole surface is not possible.

We begin with the problem of inverting the dHvA areas into radii. Assume that we have an initial set of C_j generated from a band-structure calculation. We furthermore assume that we have a set of experimental areas selected such that the electron in traveling around these orbits samples most of the Fermi surface. We would require at least as many experimental data points as the number of stars in the representation. From the initial C_j we could calculate areas corresponding to each of the experimental areas. Let A_i^e be the set of experimental areas and A_i^c be the calculated values. As a measure of the quality of the fit we define the function Δ by the relation

$$\Delta^2(C_0,C_1,\ldots,C_m)=\frac{1}{N}\sum_{i=1}^{N}(A_i^c-A_i^e)^2. \quad (11)$$

The initial C_j do not in general minimize this function. Let the values of C_j which do minimize this function be $C_j'\equiv C_j+\delta C_j$. Then we have

$$\Delta^2(C_0'\cdots C_m')=\Delta^2(C_0\cdots C_m)+\sum_{j=1}^{m}\frac{\partial\Delta^2}{\partial C_j}\delta C_j+\tfrac{1}{2}\sum_{j,l}^{m}\frac{\partial^2\Delta^2}{\partial C_j\partial C_l}\delta C_j\delta C_l. \quad (12)$$

We minimize this with respect to δC_j, obtaining

$$\frac{\partial\Delta^2}{\partial C_j}+\sum_{l=1}^{m}\frac{\partial^2\Delta^2}{\partial C_j\partial C_l}\delta C_l=0. \quad (13)$$

The above is a set of linear equations in δC_l, and the problem now is to evaluate the vector and tensor coefficients $\partial\Delta^2/\partial C_j$ and $\partial^2\Delta^2/\partial C_j\partial C_l$. Now, we have

$$\frac{\partial\Delta^2}{\partial C_j}=\frac{2}{N}\sum_{i=1}^{N}(A_i^c-A_i^e)\frac{\partial A_i^c}{\partial C_j}. \quad (14)$$

Using the laws of differentiation of implicit functions, and the fact that

$$A^c=\frac{1}{2}\int_0^{2\pi}k_\perp^2 d\theta,$$

we have[15]

$$\frac{\partial A^c}{\partial C_j}=-\int_0^{2\pi}k_\perp\left(\frac{\partial k_\perp}{\partial E}\right)_{C_j}\left(\frac{\partial E}{\partial C_j}\right)_{k_\perp}d\theta. \quad (15)$$

$\partial E/\partial C_j$ is nothing more than the sum of $e^{i\mathbf{k}\cdot\mathbf{R}}$ over all vectors in the jth star, this sum being defined as $S_j(\mathbf{k})$. Thus we have

$$\frac{\partial A^c}{\partial C_j}=-\int_0^{2\pi}\frac{k_\perp^2}{\mathbf{k}_\perp\cdot\nabla E}S_j(\mathbf{k})d\theta. \quad (16)$$

This completes the calculation of $\partial\Delta^2/\partial C_j$. Now,

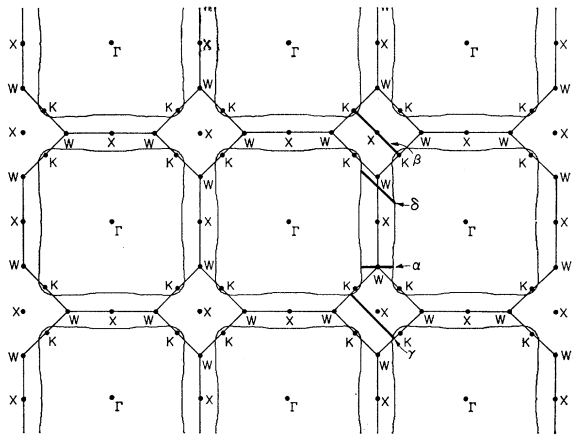

FIG. 9. ϵ orbit shown in the extended zone scheme. The positions of the α, β, γ, and δ orbits are indicated.

[15] The treatment here assumes that the plane of the orbit remains constant, i.e., the orbits include a point of sufficiently high symmetry. The generalization to the case where the orbit moves on varying C_j is straightforward.

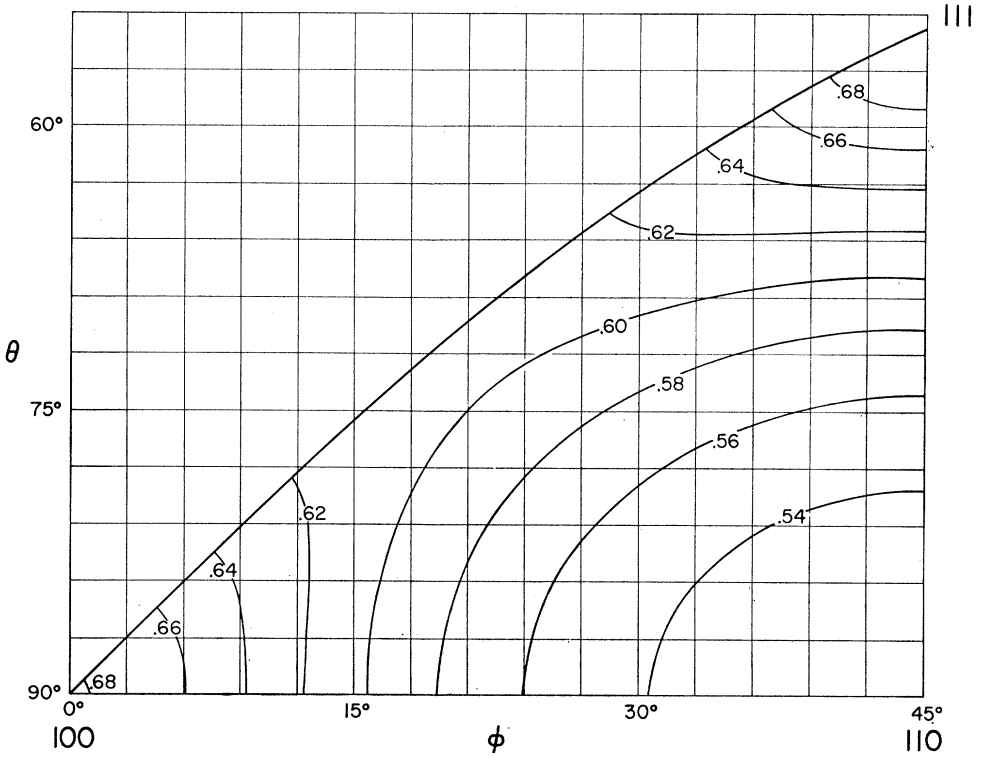

FIG. 10. Contours of constant radius for the sixth-band electron surface.

$\partial^2\Delta^2/\partial C_j\partial C_l$ is given by

$$\frac{\partial\Delta^2}{\partial C_j\partial C_l}=\frac{2}{N}\sum_{i=1}^{N}\left(\frac{\partial A_i{}^c}{\partial C_j}\frac{\partial A_i{}^c}{\partial C_l}+(A_i{}^c-A_i{}^e)\frac{\partial^2 A_i{}^c}{\partial C_j\partial C_l}\right). \quad (17)$$

The only quantity which we have not already evaluated is $\partial^2 A_i{}^c/\partial C_j\partial C_l$. A short calculation yields

$$\frac{\partial^2 A^c}{\partial C_l\partial C_j}=\int_0^{2\pi}\left(k_\perp{}^2\frac{S_l(\mathbf{k})S_j(\mathbf{k})}{(\mathbf{k}_\perp\cdot\nabla E)^2}+k_\perp{}^2\frac{S_j(\mathbf{k})\mathbf{k}_\perp\cdot\nabla S_l(\mathbf{k})+S_l(\mathbf{k})\mathbf{k}_\perp\cdot\nabla S_j(\mathbf{k})}{(\mathbf{k}_\perp\cdot\nabla E)^2}-k_\perp{}^2\frac{S_l(\mathbf{k})S_j(\mathbf{k})\mathbf{k}_\perp\cdot\nabla\nabla E\cdot\mathbf{k}_\perp}{(\mathbf{k}_\perp\cdot\nabla E)^3}\right)d\theta, \quad (18)$$

where the dyadic $\nabla\nabla E$ is given by

$$\nabla\nabla E(\mathbf{k})=-\sum_{\mathbf{R}}\mathbf{RR}C_{\mathbf{R}}{}^n e^{i\mathbf{k}\cdot\mathbf{R}}. \quad (19)$$

The important point is that a complete iteration requires going around each orbit only once. At each point in the ith orbit we calculate the contributions to the integrals for the elements of the vector $\partial A_i{}^c/\partial C_j$ and the tensor $\partial^2 A_i{}^c/\partial C_j\partial C_l$. It is also possible to extend this technique to simultaneously fit areas and effective masses.

As outlined in the calculation section above, the least-squares procedure used to fit a band-structure calculation yields a best rms fit to the energy, i.e., the value of

$$\Delta^2=\sum_{i=1}^{N}(E_i{}^c-E_F)^2$$

is minimized where $E_i{}^c$ is the calculated energy at the ith k vector. However, it would sometimes be desirable to use the C_j which yield the best rms fit to the energy as the initial values for obtaining a new set of C_j which yield a best rms fit to the radii. Obvious extensions of the techniques developed in the present section make this possible.

CONTOUR GENERATION

There are two common ways of presenting the details of the shape of the Fermi surface. One might graph the intersection of the surface with planes spaced uniformly along some axis such as the [100] axis. This is not very economical, since many such slices would be required for an accurate presentation. However, such slices are easily generated using the same techniques used to calculate dHvA orbits. The second and most economical way is to construct a contour map of the surface. We will now discuss how contours of constant radius may be generated using the Newton-Rhapson approach. To generate a contour we must be able to carry out two

operations: (1) If a vector is off the surface and off the contour, we must replace, it by one which is closer to the surface and contour; and (2) having a vector that is on the surface and on the contour, we must generate a new vector which is also on the surface and contour but which had advanced by a known angle.

We define the following four unit vectors:

$$\hat{n}_1=\nabla E/|\nabla E|\,,\quad \hat{n}_2=\mathbf{k}\times\hat{n}_1/|\mathbf{k}\times\hat{n}_1|\,,$$
$$\hat{n}_3=\hat{n}_1\times\hat{n}_2,\quad \hat{n}_4=\mathbf{k}/|\mathbf{k}|\,.$$

Consider first process (1). If we have a vector $\mathbf{k}$ which is off the surface and contour, we want to replace it by a vector $\mathbf{k}'=\mathbf{k}+\delta\mathbf{k}$ which is closer to the surface and contour. We require $\delta\mathbf{k}$ to lie in the plane formed by the vectors $\hat{n}_1$ and $\hat{n}_3$, i.e.,

$$\delta\mathbf{k}=a\hat{n}_1+\ b\hat{n}_3.$$

The values of a and b are found using Eq. (6) together with the condition $k_0^2=|\mathbf{k}+\delta\mathbf{k}|^2\cong k^2+2\mathbf{k}\cdot\delta\mathbf{k}$, where k_0 is the radius of the contour under consideration. The result is

$$a=\frac{E_F-E(\mathbf{k})}{|\nabla E|}$$

and

$$b=\frac{1}{\hat{n}_3\cdot\mathbf{k}}\left(\frac{k_0^2-k^2}{2}-\frac{E_F-E(\mathbf{k})}{|\nabla E|}\hat{n}_1\cdot\mathbf{k}\right).$$

We repeat this process until $\delta k/k$ is smaller than some specified number (0.001, in our case). Now consider process (2). Having a vector $\mathbf{k}$ which is on the surface and contour, we wish to replaced it with a vector $\mathbf{k}'=\mathbf{k}+\delta\mathbf{k}$ which is quite close to the surface and contour but which makes an angle θ with $\mathbf{k}$. We require $\delta\mathbf{k}$ to lie in the plane formed by the vectors $\hat{n}_2$ and $\hat{n}_4$. A short calculation shows that

$$\delta\mathbf{k}=2k\,\sin\tfrac{1}{2}\theta(\hat{n}_2\cos\tfrac{1}{2}\theta\ -\hat{n}_4\sin\tfrac{1}{2}\theta)\,.$$

By alternatively applying operations (1) and (2), we may advance around a contour of constant radius. Figure 10 shows the contours of constant radius for the Γ-centered surface of platinum.

PHYSICAL REVIEW VOLUME 186, NUMBER 3 15 OCTOBER 1969

Point-Defect Interactions in Elastic Materials of Grade 2

WILLIAM F. ADLER
Battelle Memorial Institute, Columbus Laboratories, Columbus, Ohio 43201
(Received 8 May 1969)

The main result of this paper is that two centers of dilatation in an infinite, isotropic domain do possess an interaction energy according to the linearized version of Toupin's strain-gradient theory of elasticity—in contrast to the classical theory of elasticity, where the interaction energy was shown to be zero. The center of dilatation has been adopted by many investigators as a representation of point defects in crystalline solids, so the above result may have significance in evaluating the long-range interactions which may occur between point defects.

I. INTRODUCTION

THE classical theory of elasticity has been used by a number of authors to study the behavior of point defects and dislocations in crystalline solids. While this approach admittedly may not be appropriate in a number of cases to which it has been applied, it has yielded several useful results. In order to simplify the analysis the crystalline solid is assumed to be isotropic and infinite in extent. Within this general framework the present paper applies a recently developed, nonclassical theory of elasticity to the problem of the interaction of two centers of dilatation in an infinite, isotropic, elastic medium. In contrast to the statement which is frequently made, based on the work of Bitter,[1] that the interaction energy of two centers of dilatation in an infinite, isotropic, elastic medium is zero, an explicit expression for the interaction energy will be given. This seems to be more in line with the results obtained from digital-computer computations based on lattice models. The classical result has been especially noted and criticized by Hardy and Bullough.[2]

A number of investigators have considered generalizations of the fundamental model of a continuum which forms the basis of the classical theory of elasticity. The generalized continuum models have the common feature that they take into account more of the details around a material point. There is evidence that the generalized continuum models may incorporate some of the lattice characteristics of crystalline solids in the continuum approach. However, most of the nonclassical theories are in their early stages of development, so it is still somewhat premature to judge the potential value of these new models.

[1] F. Bitter, Phys. Rev. **35**, 1527 (1931).

[2] J. R. Hardy and R. Bullough, Phil. Mag. **15**, 237 (1967).

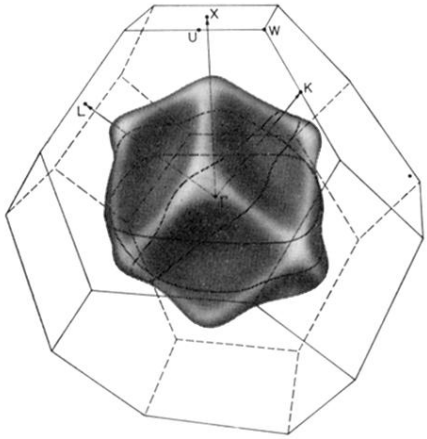

FIG. 1. Sixth-band electron surface in Pt calculated using the interpolation scheme.

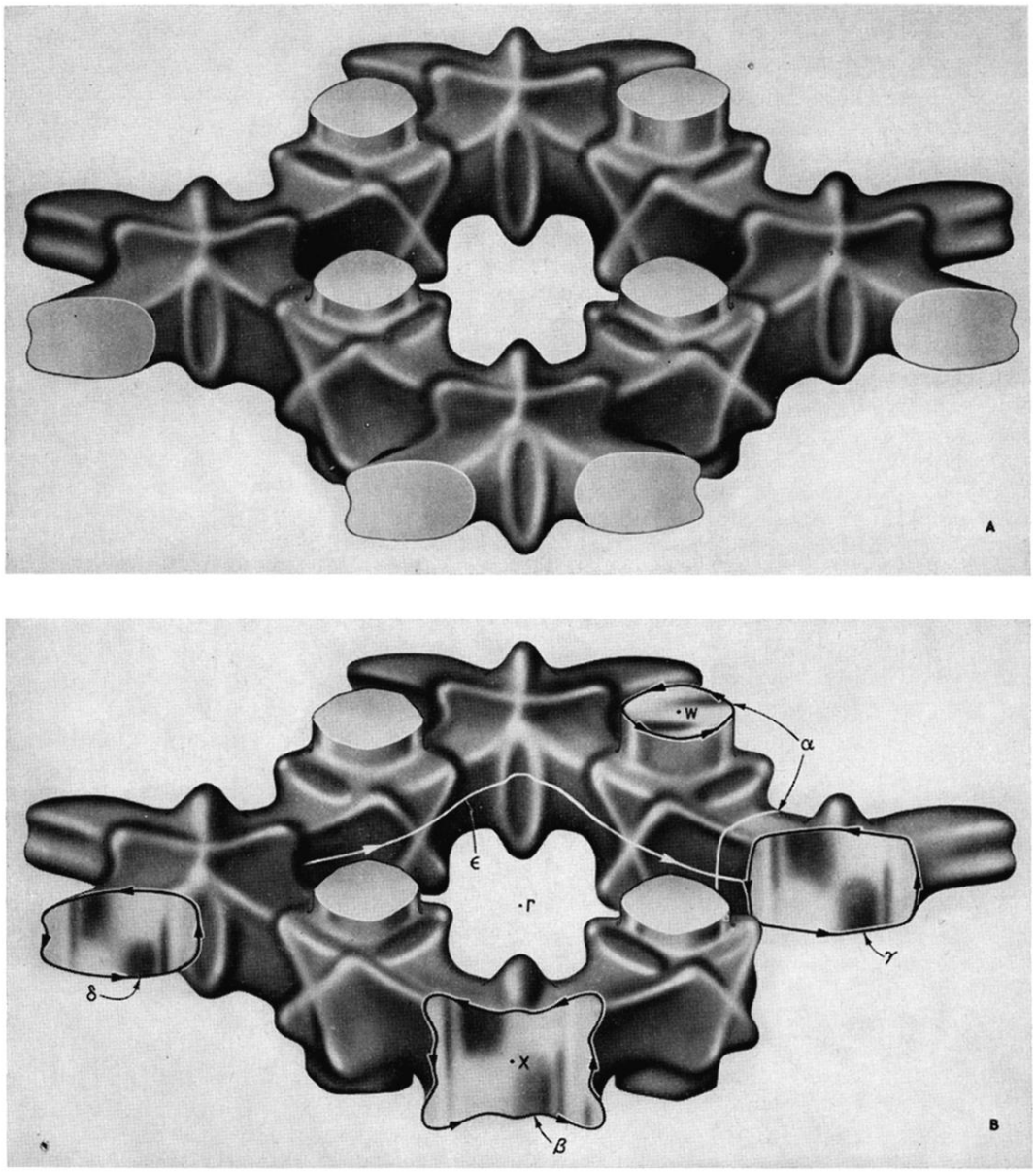

FIG. 2. (a) Open fifth-band hole surface in Pt calculated using the interpolation scheme; (b) open fifth-band hole surface in Pt showing the expected dHvA orbits.